Third-order spatial correlations for ultracold atoms

2013 New J. Phys. 15 013042

(http://iopscience.iop.org/1367-2630/15/1/013042)

New Journal of Physics
The open access journal for physics

Third-order spatial correlations for ultracold atoms

A G Manning, Wu RuGway, S S Hodgman, R G Dall, K G H Baldwin and A G Truscott[1]

Australian Centre for Quantum-Atom Optics, Research School of Physics and Engineering, Australian National University, Canberra, ACT 0200, Australia
E-mail: andrew.truscott@anu.edu.au

New Journal of Physics **15** (2013) 013042 (10pp)
Received 15 October 2012
Published 18 January 2013
Online at http://www.njp.org/
doi:10.1088/1367-2630/15/1/013042

Abstract. We present here the first measurement of the third-order spatial correlation function for atoms, made possible by cooling a metastable helium cloud to create an ultracold thermal ensemble just above the Bose–Einstein condensation point. The resulting large correlation length well exceeds the spatial resolution limit of the single-atom detection system, and enables extension of our earlier temporal measurements to evaluate the third-order correlation function in the spatial plane of the detector. The enhancement of the spatial third-order correlation function above a value of unity demonstrates the presence of spatial three-atom bunching, as expected for an incoherent source.

Contents

[1] Author to whom any correspondence should be addressed.

1. Introduction

The coherence of a light source can be characterized by determining the statistical distribution of the time of arrival between photons from the source, as described theoretically by Glauber [1]. For pairs of photons, the normalized second-order correlation function is defined as the arrival probability of a second photon as a function of the delay following the detection of the first photon, normalized by the individual photon probabilities. Likewise, the third- and higher-order correlation functions are obtained from the arrival times between triplets and larger groups of photons.

A perfectly coherent source is characterized by a uniform arrival probability, yielding a correlation function of unity for all orders. By contrast, a thermal (incoherent) light source is characterized by photon bunching, whereby the probability of detecting groups of photons at short delay times is higher than at long delay times. Theoretically, the maximum bunching enhancement factor for the nth-order correlation function is $n!$ at zero delay time [1], but this may be significantly reduced in experimental measurements due to the finite resolution of the detection system. However, provided that the detector temporal resolution is significantly smaller than the width of the bunching signal, then the bunching width corresponds to the correlation time of the source.

An early experiment by Hanbury Brown and Twiss [2] measured for the first time the second-order correlation function of an incoherent light source and demonstrated two-photon bunching. The same measurement can be applied in the spatial domain, where the probability of pairs of photons with particular spatial (rather than temporal) separations is measured. Applying this to stellar light sources, Hanbury Brown and Twiss [3] were able to measure the second-order spatial correlation function to determine the angular width of stars. Their pioneering experiments represent the early foundations of quantum optics.

The same concepts apply to particles—including atoms—where in addition both bosonic and fermionic species exist (cf bosonic photons). Second-order correlation functions have been determined for both incoherent (thermal) sources [4] and coherent (Bose–Einstein condensate(BEC)) atomic sources [5]. Thermal and BEC sources exhibited bunching and unity correlation values respectively, with antibunching being demonstrated for fermions [6, 7].

However, until recently, there has been no matter-wave experimental verification of Glauber's conjecture that coherent sources exhibited unity correlation functions to higher order. Using a new experimental technique in our laboratory, we were able to make the first measurements of the third-order correlation function [8] which demonstrated temporal three-atom-bunching for a thermal gas of ultracold bosonic helium, and a correlation value of unity for a BEC. This result is consistent with BECs being characterized by coherence to higher orders, in the same way that an optical laser is higher-order coherent. More recently, temporal correlations up to fourth order have been measured for trapped thermal atoms [9].

In subsequent experiments using ultracold helium atoms guided in multiple modes of an all-optical waveguide [10], we were able to demonstrate the connection between the first observation of spatial atomic speckle and temporal two-atom bunching [11], both characteristic of second-order incoherence. This correspondence between spatial and temporal correlations is to be expected from Glauber's formalism as was demonstrated for photons by Hanbury Brown and Twiss. In similar experiments using atoms, second-order spatial correlation measurements have also demonstrated atom bunching [5]. Spatial auto-correlation measurements have yielded similar information about the spatial structure of the ensemble [12–16].

Experiments determining the third-order spatial correlation function have thus far only been performed using photons, whereby three separate point detectors were used to measure the spatial coincidence of photon triplets [17]. The simulated (and experimental) results show that the probability of jointly detecting three randomly radiated photons from a chaotic thermal source using three separate detectors is 6 (and ∼5) times greater if the events fall within the coherence time and volume of the radiation field. The imperfect three-photon-bunching enhancement is attributed to the finite detector resolution.

In this paper, we apply a similar concept to measure the third-order spatial correlation function of an atomic ensemble for the first time. (Other experiments have indirectly measured the effect of third-order correlations on collision processes [18–20].) The significance of spatial correlation measurements is fourfold.

Firstly, for an isotropic (three-dimensional spatially symmetric) cloud of atoms, spatial coherence measurements can—interchangeably with temporal coherence measurements—be used as a diagnostic for the overall coherence properties of the ensemble. Secondly, in situations where there is a constrained dimensionality of the system e.g. for atoms confined in one-dimensional and two-dimensional trapping geometries, the measurement of the spatial correlation functions in each trapping dimension can provide additional information on the coherence properties of the atomic source [15]. Thirdly, higher-order spatial correlations can be used to enhance image visibility, such as in the photon experiments undertaken in [17]. There the authors also perform a 'ghost imaging' experiment using three-photon coincidences, and show that the visibility is significantly improved over similar experiments performed using two-photon coincidences.

Fourthly, while the formalism developed by Glauber [1] indicates that third-order correlation functions can be expressed via Wick's theorem in terms of lower order correlation functions (see supplementary online materials in [8]), the third-order correlation functions can be related directly to processes involving three-body physics. This includes three-body collisions (such as studied in [18–20]), and Efimov physics where stable three-body bound states can exist even when two-body interactions are too weak to create pairing [21–23]. Spatial third-order correlation measurements are therefore of interest in their own right through the elucidation of three-body physics, as well as for the information provided on the overall coherence, geometric dimensionality and imaging resolution.

2. Experiment

Here, we extend our measurements of spatial first-order coherence from the matter-wave imaging techniques employed previously [10], to enable single-atom measurements that yield both second- and third-order correlation functions in the spatial domain. We employ metastable helium atoms (He^*) in the 2^3S_1 state which has a very long lifetime (∼8000 s [24]) and which lies ∼20 eV above the ground state enabling efficient single atom detection [25]. We use the same apparatus as employed earlier to create a He^* BEC [26] and a pulsed He^* atom laser [27] to generate a cloud of ultracold He^* atoms.

In our previous temporal third-order correlation experiments [8] we used multiple radio-frequency (RF) output coupling pulses to create a large number of thermal samples just above the relatively high (∼1 μK) critical temperature T_c for BEC formation. (The temperature is determined by measuring the time-of-flight distribution of atoms released from the trap, with

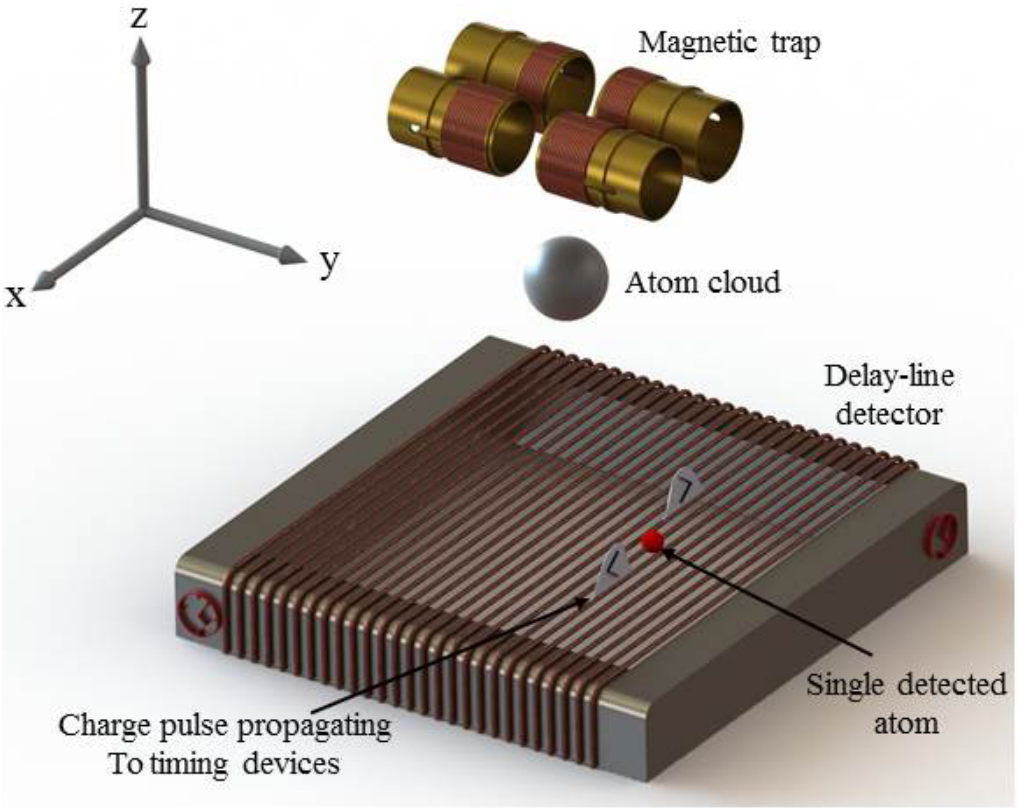

Figure 1. Experimental schematic. After release from the magnetic trap, the expanding cloud of ultracold He^* atoms falls under gravity onto the MCP. The amplified electron pulse from a single detection event on the MCP is incident upon the DLD wire (shown only for the x-axis) which creates a current pulse whose arrival time at each end of the wire then provides the spatial location in that dimension.

the uncertainty dominated by shot-to-shot fluctuations.) However, in the current experiments we progressively evaporatively cool the atoms in the magnetic trap to much lower temperatures ($\sim$100 nK) in order to increase the correlation length to minimize the effects of detector resolution, while at the same time increasing the probability for detecting pairs of atoms within the spatial correlation length.

The starting point is a bi-planar quadrupole Ioffe configuration (BiQuic) magnetic trap [26] shown schematically in figure 1, which has trapping frequencies in the x, y and z (or equivalently time) direction of 50, 550 and 550 Hz respectively. We load atoms into the trap, and continuously evaporatively cool the atoms using a swept RF field to just above T_c yielding $\sim 10^6$ atoms at a temperature of $\sim 1\ \mu$K. At this point, the correlation length is of order the spatial resolution of the detector ($\sim 150\ \mu$m [8]). The correlation length at the detector l^d scales linearly with the time t taken for the atoms to drop from the trap to the detector, and is given by [28]

$$l^d = \hbar t / m s^t, \tag{1}$$

where m is the particle mass and s^{t} is the size of the cloud in the trap

$$s^{\mathrm{t}} = (k_{\mathrm{B}}T/m\omega^2)^{1/2} \tag{2}$$

for trap temperature T, frequency ω and Boltzmann constant k_{B}. By comparison, the transverse de Broglie wavelength in trap is given by $\lambda_{\mathrm{dB}} = h/mv_{\mathrm{trans}} \sim l^{\mathrm{d}}(2\pi/t\omega)$.

To increase the correlation length, we continue the evaporative cooling process to reduce the temperature (and hence the trap size) while simultaneously smoothly attenuating the atom number to avoid condensation. The attenuation is achieved during the final 2.7 s of the evaporation process by using additional broadband RF pulses (with a 50% duty cycle over a 100 μs pulse width) to remove atoms uniformly over the entire ensemble. This expels the vast majority of atoms from the trap, leaving a very cold cloud ($\sim$95 + 10 nK) of $\sim$1000 atoms, whose minimum temperature is limited by the stability of the (already highly-stablized) magnetic trap [30]. The correlation length at the detector along the y-axis is then $\sim$1.5 mm which is an order of magnitude larger than the detector resolution.

The magnetic trap is then switched off, thereby releasing the atoms which fall $\sim$848 mm over 416 ms under gravity onto an 80 mm diameter micro-channel plate (MCP) detector. By optimizing the evaporation process, we can achieve a highly reproducible ensemble number which yields $\sim$350 detection events per experimental cycle, which are then averaged over nearly 4000 cycles.

As the He* atoms arrive at the MCP their $\sim$20 eV internal energy creates an electron pulse which is then incident upon a delay-line detector (Roentdek DLD80). The DLD consists of a wire coil in both the x and y dimensions (figure 1) in which a current pulse is generated for each MCP event. By measuring the arrival time at the end of each wire the three-dimensional position of the detection event can be reconstructed.

The detector spatial resolution ($\sim$150 μm) is set by a combination of the MCP pore size and the DLD detection electronics. The detector resolution was determined by passing He* atoms through a fiducial mask which acts as a point source of atoms. The point spread function determined by the system geometry was then deconvolved from the resulting image to obtain the detector resolution.

The correlation functions are then determined using a similar technique to that described in [8], except that here we measure correlations in the plane of the detector (defined by the x- and y-axis in figure 1) rather than in time (or its equivalent, the z-axis). For a spherical trap the isotropic nature of the expanding atomic cloud yields the same correlation length at the detector along both axes. However, in our system, the difference in the x- and y-axis trapping frequencies (50 and 550 Hz respectively) yields more than an order-of-magnitude greater correlation length in the y-direction. Since the x-axis correlation length is of order the detector resolution, we have concentrated on measuring the y-axis correlation function.

A detection event is analysed to determine whether another event occurs within a given spatio-temporal bin to determine $g^{(2)}(\Delta y)$. The bin size used was 250 μs in the z-direction (corresponding to $\Delta z = 1$ mm at a velocity of 4 m s^{-1}), 1 mm in the x-direction and 200 μm in the y-direction. The x, y, t bin sizes need to be at least as large as the detector resolution, and the smaller y bin size reflects the optimization of the data sets needed to achieve the best signal-to-noise ratio. To measure the third-order spatial correlation function $g^{(3)}(\Delta y_1, \Delta y_2)$, the data is analysed to determine whether a further particle arrives within the same bin volume centred on the second particle position.

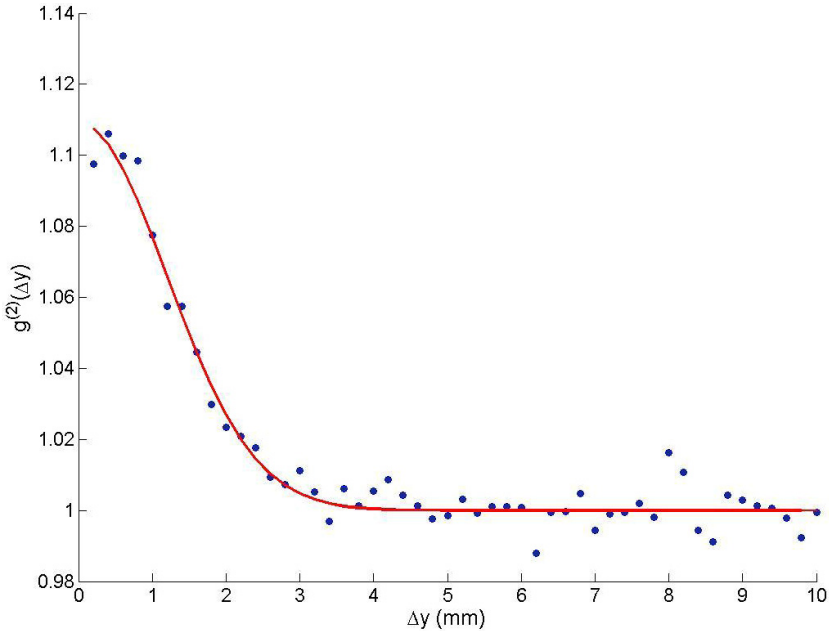

Figure 2. Normalized second-order spatial correlation function $g^{(2)}(\Delta y)$ for $\sim$95 nK thermal atoms. The red line shows a gaussian fit to the data.

3. Results

The second-order correlation function $g^{(2)}(\Delta y)$ determined by this process is shown in figure 2 for a thermal ensemble at $\sim$95 nK. Here the clear atom bunching signature can be seen at small particle separations, with a correlation length of 1.30 ± 0.03 mm. The bunching enhancement factor is 1.131 ± 0.015 compared with the expected value of 2.0 (2!) given perfect detector resolution. A simple theoretical model [8] using our experimental values with no free parameters predicts an enhancement of 1.14 ± 0.02 and a correlation length of 1.5 ± 0.2 mm, in good agreement with the experiment.

The simple theoretical model is the same as employed in our previous experiment [8, supplementary online material] and is based on the method of Gomes *et al* [28] which employs the theory of Naraschewski and Glauber [29]. The theory allows the determination of $g^{(2)}(\Delta y)$ at the detector for a trapped atomic cloud released in the absence of interparticle interactions (which applies at our very low atomic number densities). The correlation function depends on the cloud temperature, the trap frequencies, and the time taken for the atoms to fall under gravity from the trap to the detector, all of which we determine empirically from the experiment. The model can also be extended to higher order correlation functions via Wick's theorem.

However, the finite experimental resolution will reduce the peak bunching amplitude to a value less than $n!$—the ideal value for the nth order correlation function for incoherent bosons. In addition to the finite detector spatial resolution ($\sim$150 μm), as indicated above the data is binned along the various axes to improve the signal-to-noise-ratio, and if the bin size comparable to or greater than the correlation length, it will also contribute to a loss of resolution.

The correlation functions determined using [28] are averaged over the bin volume where the position of each detected atom is degraded by the detector resolution. The reduction in bunching amplitude is dominated by this imperfect resolution, which can be approximated by

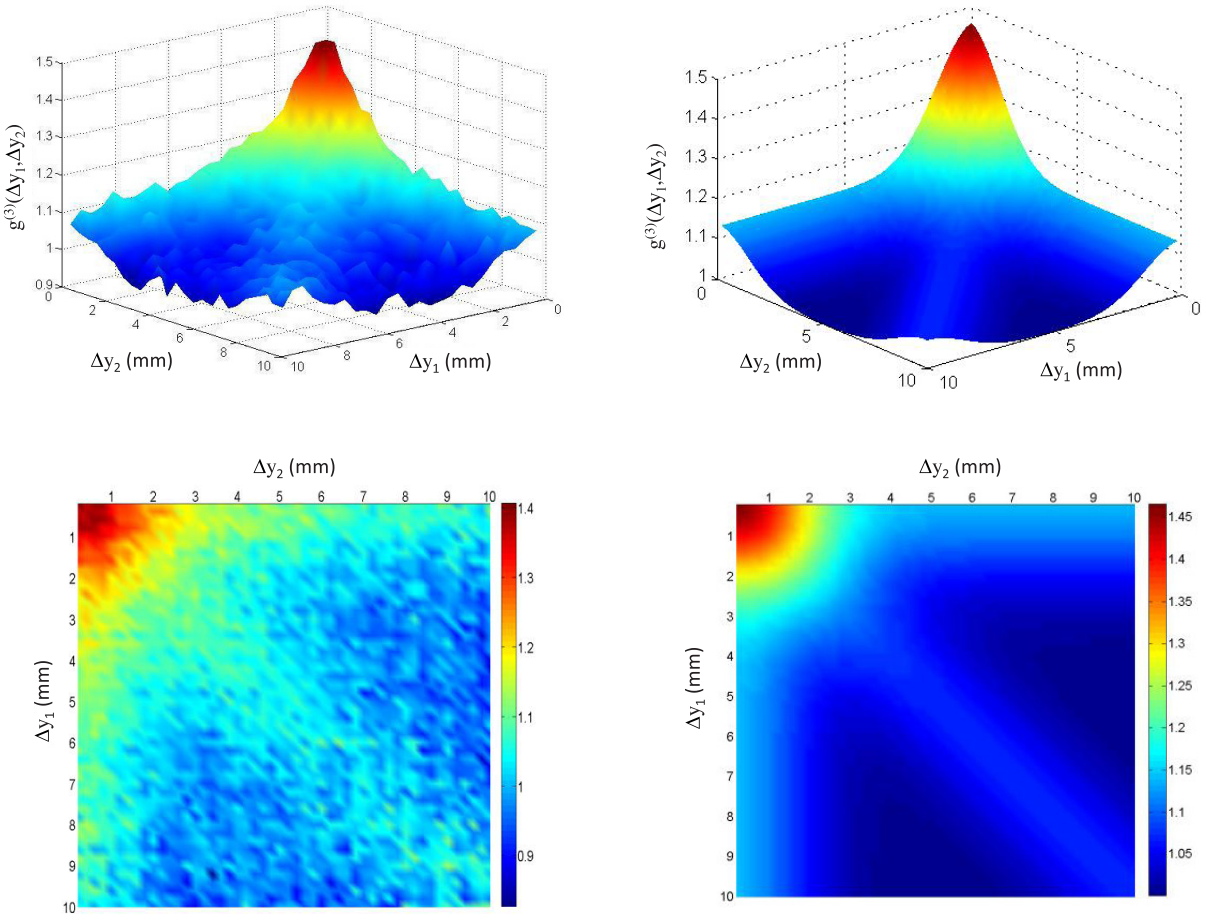

Figure 3. Normalized third-order spatial correlation functions $g^{(3)}(\Delta y_1,\ \Delta y_2)$ (top left). Three-dimensional plot of the experimental data with false colour rendering (top right). Corresponding theory obtained from our simple model (bottom). Plan view of the both images. Note the diagonal ridge corresponding to the enhanced probability of both particles 2 and 3 being present at the same Δy value.

convoluting the correlation function with a single Gaussian function that represents the effective resolution (the combination of bin size and detector resolution) so that the peak bunching for second order becomes

$$g^{(2)}_{\mathrm{obs}} = 1 + \prod_{\alpha\in(x,y,z)} \sqrt{\frac{(1+d_\alpha^2/S_\alpha^2(t))}{\left(1+4d_\alpha^2/\left(l_\alpha^{\mathrm{d}}\,(t)\right)^2\right)}}, \tag{3}$$

where $l_\alpha^{\mathrm{d}}(t)$ is the correlation length at the detector, $S_\alpha(t) = t^*(k_{\mathrm{B}}T/m)^{1/2}$ is the cloud size at detector, and d_α is the effective rms resolution. To further improve this, corrections are added to represent the response of the MCP and DLD system and temperature fluctuations using a Monte Carlo method to average the correlation functions over the three-dimensional effective bin volume. The resulting model therefore has no free parameters as all the variables are determined directly from the experiment.

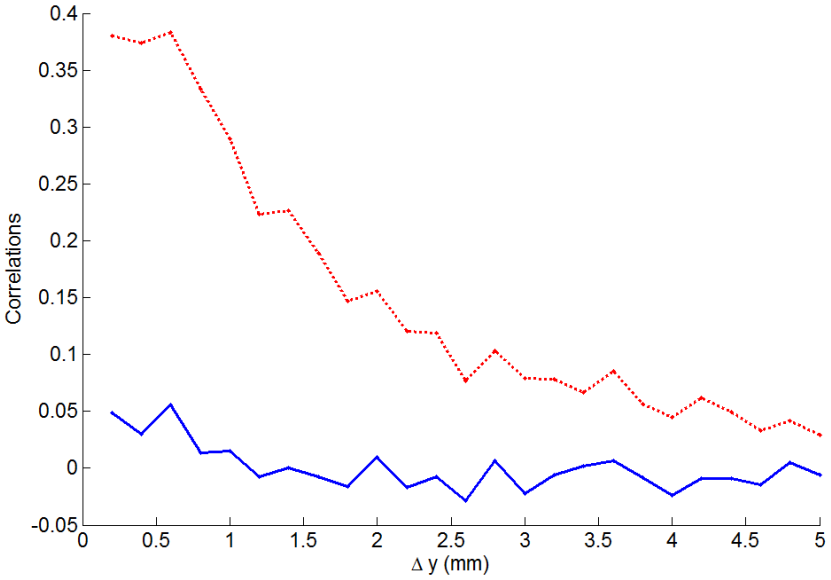

Figure 4. Plot of $g^{(3)}(\Delta y_1 = \Delta y_2 = \Delta y) - 1$, red dashed line, and the three-body contribution, blue solid line, to $g^{(3)}(\Delta y_1 = \Delta y_2 = \Delta y)$.

The measured third-order correlation function $g^{(3)}(\Delta y_1,\ \Delta y_2)$ is shown in figure 3 (top left). This is plotted as a function of the y-axis separation for each particle pair in the triplet i.e. $\Delta y_1 = y_2 - y_1$ and $\Delta y_2 = y_3 - y_2$. The measured bunching enhancement is 1.44 ± 0.02 compared with an expected enhancement of 6.0 (3!) with perfect detector resolution. The simple theoretical model [8] with no free parameters yields 1.47 ± 0.05 (top right). A plan view of both the three-dimensional plot is also shown in the plots underneath. Note that the second-order correlation function in figure 2 can in principle be derived from the third-order function in figure 3 when one atom is a large distance from the other two in each triplet (for example, $g^{(2)}(\Delta y_1)$ can be found by averaging $g^{(3)}(\Delta y_1,\ \Delta y_2)$ for values of Δy_2 much greater than the correlation length).

Apparent in all the three-dimensional and plan views is a ridge of enhancement along the diagonal, where the separation of the first and third particles from the second is the same. This is to be expected, as when $\Delta y_1 = \Delta y_2$ there is an enhanced probability of two of the three particles being close together and therefore interfering.The same phenomenon is present in the third-order spatial correlation measurements using photons reported in [17]. This ridge line is not present in the temporal third-order correlation function presented in [8] since time-ordering is implicit in the detection of particle three after the detection of a particle pair (allowing intervals without time ordering i.e. enabling time reversal of the first two particles, would yield the same diagonal ridge).

Finally, it is interesting to note that $g^{(3)}$ contains contributions from $g^{(2)}$ since (as noted above) when one of the three particles is taken far away, $g^{(3)}$ reduces to $g^{(2)}$. It is possible to remove these two-body contributions from the three-body correlation function (see equation S2 in the – supporting online material [8]). Such a decomposition has been used previously for ultracold atoms [31] and weakly correlated plasmas [32]. Figure 4 shows the three-body correlation function ($g^{(3)}(\Delta y_1 = \Delta y_2 = \Delta y) - 1$, dashed red line) as well as the contribution towards this signal from solely three-particle interference (solid blue line).

4. Conclusion

Using an improved experimental technique, we have extended our temporal third-order correlation measurements to determine the spatial third-order correlation function for atoms for the first time. By reducing the temperature of the atomic cloud by over an order of magnitude to ∼95 nK, we have been able to increase the correlation length in the y-direction to more than an order of magnitude greater than the spatial resolution of the detector. This also increases the number of pair and triplet events measured within the bin size, despite the reduction in the number of atoms detected as a result of the evaporative cooling process.

The result is a large enhancement of the spatial atom-bunching signal values of 1.131 ± 0.015 for $g^{(2)}(\Delta y)$ and 1.44 ± 0.02 for $g^{(3)}(\Delta y_1, \Delta y_2)$, compared with 1.022(2) and 1.061(6) respectively for the temporal second- and third-order correlations measured previously [8]. This strong atom-bunching signal is a clear signature of the incoherent nature of the thermal atomic ensemble.

The measurement of higher-order spatial correlation functions in atomic ensembles holds promise for enhancing imaging visibility [17], and for probing quantum mechanical phenomena such as entanglement and the violation of Bell's inequalities [33]. By improving our correlation techniques to increase the atom-bunching signals, we aim to make higher-order correlation measurements more accessible for such applications.

Acknowledgments

The authors would like to acknowledge the support of the Australian Centre for Quantum-Atom Optics. AGT acknowledges the support of the Australian Research Council through the Future Fellowship programme.

References

[1] Glauber R J 1963 *Phys. Rev.* **130** 2529
[2] Hanbury Brown R and Twiss R Q 1956 *Nature* **177** 27
[3] Hanbury Brown R and Twiss R Q 1956 *Nature* **178** 1046
[4] Yasuda M and Shimizu F 1996 *Phys. Rev. Lett.* **77** 3090
[5] Schellekens M *et al* 2005 *Science* **310** 648
[6] Rom T *et al* 2006 *Nature* **444** 733
[7] Jeltes T *et al* 2007 *Nature* **445** 402
[8] Hodgman S S *et al* 2011 *Science* **331** 1046
[9] Guarrera V *et al* 2011 *Phys. Rev. Lett.* **107** 160403
[10] Dall R G *et al* 2011 *Optics Letters* **36** 1131
Dall R G *et al* 2010 *Phys. Rev.* A **81** 011602
[11] Dall R G *et al* 2011 *Nature Commun.* **2** 291
[12] Hellweg D *et al* 2003 *Phys. Rev. Lett.* **91** 010406
[13] Fölling S *et al* 2005 *Nature* **434** 481
[14] Greiner M *et al* 2005 *Phys. Rev. Lett.* **94** 110401
[15] Manz S *et al* 2010 *Phys. Rev.* A **81** 031610
[16] Perrin A *et al* 2012 *Nature Phys.* **8** 195
[17] Zhou Yu *et al* 2010 *Phys. Rev.* A **81** 043831
[18] Burt E A *et al* 1997 *Phys. Rev. Lett.* **79** 337

[19] Laburthe Tolra B *et al* 2004 *Phys. Rev. Lett.* **92** 190401
[20] Haller E *et al* 2011 *Phys. Rev. Lett.* **107** 230404
[21] Kraemer T *et al* 2006 *Nature* **440** 315
[22] Knoop S *et al* 2009 *Nature Phys.* **5** 227
[23] Zaccanti M *et al* 2009 *Nature Phys.* **5** 586
[24] Hodgman S S *et al* 2009 *Phys. Rev. Lett.* **103** 053002
[25] Vassen W *et al* 2012 *Rev. Mod. Phys.* **84** 175
[26] Dall R G and Truscott A G 2007 *Opt. Commun.* **270** 255
[27] Manning A G *et al* 2010 *Opt. Express* **18** 18712
[28] Gomes J V *et al* 2006 *Phys. Rev.* A **74** 053607
[29] Naraschewski M and Glauber R J 1999 *Phys. Rev.* A **59** 4595
[30] Dedman C J *et al* 2007 *Rev. Sci. Instrum.* **78** 024703
[31] Armijo J *et al* 2010 *Phys. Rev. Lett.* **105** 230402
[32] Boyd T J M and Sanderson J J 2003 *The Physics of Plasmas* (Cambridge: Cambridge University Press)
[33] Jack B *et al* 2009 *Phys. Rev. Lett.* **103** 083602